ADVANCED OPTICAL MATERIALS
www.advopticalmat.de

Materials Views
www.MaterialsViews.com

N,S-Induced Electronic States of Carbon Nanodots Toward White Electroluminescence

Sungan Do, Woosung Kwon, Young-Hoon Kim, So Rang Kang, Taehyung Lee, Tae-Woo Lee, and Shi-Woo Rhee**

In this work, nitrogen and sulfur-doped carbon nanodots (CNDs) have been synthesized from ethylenediamine-*N,N′*-diacetic acid and 2,2′-(ethylenedithio) diacetic acid, respectively. The method used in this work features the use of "single" molecular precursors that contain both carbon and dopant atoms, which allows examining the effects of doping in a molecular level. The effects of doping on the electronic structure of CNDs could be examined by a series of spectroscopic measurements including UV–vis absorption and photoluminescence. It is found that doping gives rise to new light absorption and photoluminescence bands at around 500 nm. Finally, light-emitting diodes (LEDs) with the CNDs synthesized have been demonstrated to show that the electronic states induced by direct doping influence their electroluminescence. Such LEDs successfully exhibit broadband electroluminescence covering the visible light range from 500 to 700 nm, resulting in bright pure white light whose CIE (Commission Internationale d'Éclairage) coordinate is (0.2894, 0.3351).

1. Introduction

Carbon nanodots (CNDs) are fluorescent paracrystalline zero-dimensional carbon nanoparticles with a mean diameter below 10 nm.[1,2] In contrast to conventional semiconductor nanocrystals, they have superior properties, e.g., low cost, biocompatibility, low toxicity, photostability, etc., so they have attracted much attention in optoelectronics, photocatalysis, and bioimaging.[3–7] So far, many methods have been developed for the preparation of CNDs, including laser ablation,[8] chemical oxidation,[9] electrochemical treatment,[10] thermal pyrolysis,[11–14] and microwave. Through these methods, CNDs have been obtained; however, there are still numerous challenges in improving their optical properties such as the lack of visible light absorption, blue-biased light emission, and so on.

S. Do, Dr. W. Kwon, S. R. Kang, T. Lee, Prof. S.-W. Rhee
Department of Chemical Engineering
Pohang University of Science & Technology (POSTECH)
77 Cheongam-ro, Nam-gu
Pohang 790-784, South Korea
E-mail: srhee@postech.ac.kr
Y.-H. Kim, Prof. T.-W. Lee
Department of Materials Science and Engineering
Pohang University of Science & Technology (POSTECH)
77 Cheongam-ro, Nam-gu, Pohang 790-784, South Korea
E-mail: twlee@postech.ac.kr

DOI: 10.1002/adom.201500488

Generally, the optical properties of CNDs are directly related to their electronic structure. It has been reported that the electronic structure of CNDs originates from their polyaromatic carbon domains, defective states, and surface states, presumably due to auxochromic effect.[7,15–17] Currently, doping heteroatoms, especially nitrogen and/or sulfur, in a carbon framework has been found to be an attractive strategy to control photoluminescence (PL) of CNDs.[18–38] Such dopants can be considered to generate defective states, where their different electronegativity, lone pairs of electrons, etc., change the electronic structure of CNDs. Many research groups have attempted to synthesize a variety of heteroatom-doped CNDs with distinguished optical properties. For example, Dong's group produced highly luminescent nitrogen and sulfur co-doped carbon-based dots through a one-step hydrothermal treatment using L-cysteine and citric acid as a dopant and carbon precursor, respectively.[37] In another study, Li et al. reported a facile method to prepare sulfur-doped graphene quantum dots for tuning their electronic structure by using sulfuric acid and fructose as a sulfur and carbon precursor, respectively.[38] Although these attempts have proven themselves promising; however, there have been limitations on the control of a degree of doping because heating a physical mixture of two separated precursors that have different structures and reactivity cannot guarantee the formation of desired chemical bondings between them. In this case, the bonding state of dopant atoms cannot be clear to make their roles in CNDs ambiguous. Thus, it is necessary to use a new precursor carrying both dopant and carbon atoms to not only guarantee efficient doping but also examine the effect of doping on the optical properties of CNDs in a molecular level.

Herein, we now present the synthesis of nitrogen and sulfur-doped CNDs (denoted as N-CNDs and S-CNDs, respectively) with single molecular precursors: ethylenediamine-*N,N′*-diacetic acid (EDDA) and 2,2′-(ethylenedithio)diacetic acid (ETDA), respectively.[7,12] Our doping would lead to significant changes in the electronic structure of CNDs and give rise to broad light absorption and strong PL in a long-wavelength visible light region. We finally demonstrated light-emitting diodes (LEDs) with our CNDs to show the effects of doping on their electronic structure and related electroluminescence (EL). Our

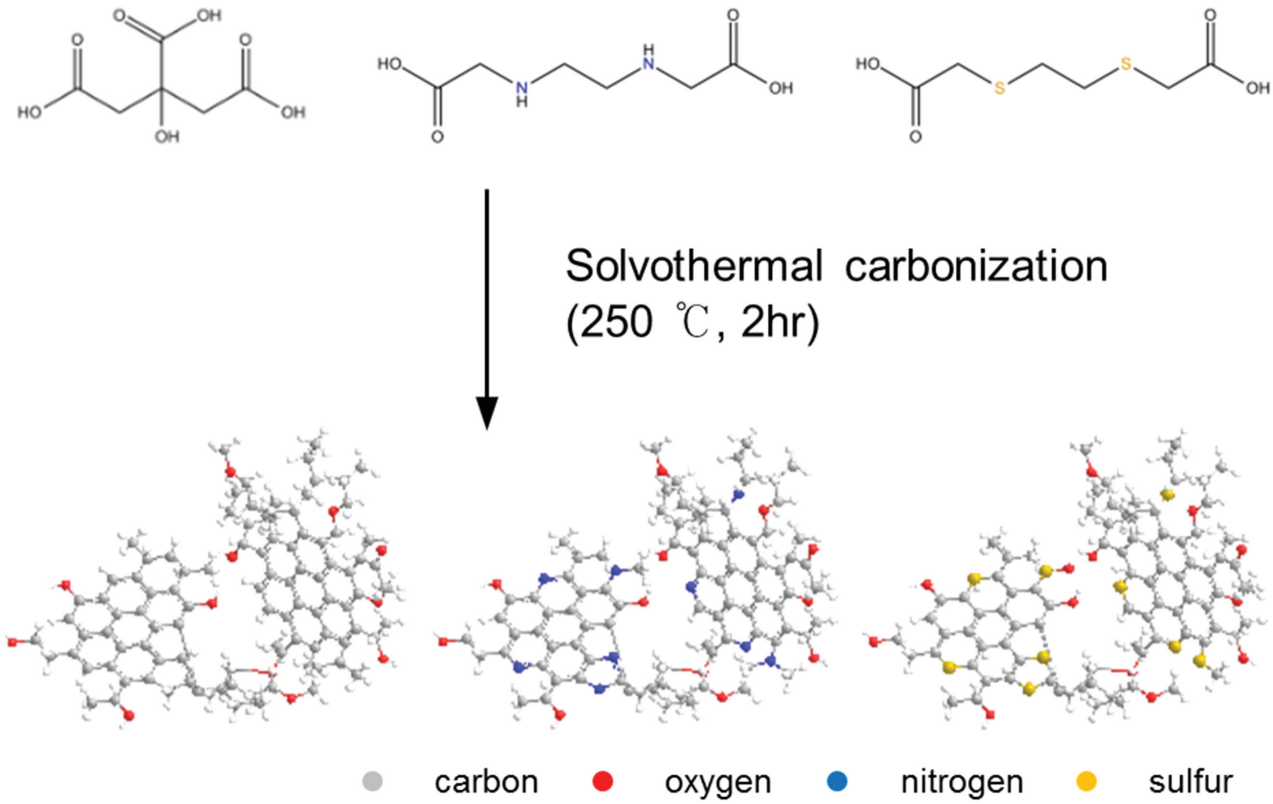

Figure 1. The schematic illustration of the synthesis of R-CNDs, N-CNDs, and S-CNDs.

results indicate that heteroatoms in a carbon framework play a very major role in changing the electronic structure of CNDs because of their chemical properties such as electronegativity, lone pair of electron, etc., different from carbon atoms.

2. Results and Discussion

2.1. Synthesis of R-CNDs, N-CNDs, and S-CNDs

In our approach, reference (R) CNDs, N-CNDs, and S-CNDs were synthesized by the solvothermal carbonization of citric acid, EDDA, and ETDA, respectively, with oleylamine as a capping agent, as illustrated in **Figure 1**. Previously, our group reported the synthesis of oleylamine-capped CNDs based on a "water-in-oil" emulsion as a self-assembled soft template.[7] Detailed synthetic method is provided in the Experimental Section. The precursors were dehydrated and carbonized by thermal energy, forming angstrom-sized polyaromatic carbon domains.[39]

2.2. Physical Properties of CNDs

To understand the physical structures of CNDs, transmission electron microscopy (TEM) was conducted. In **Figure 2**, TEM images show that no physical change was led in CNDs by doping. Figure 2a–c reveals that our CNDs were uniformly dispersed without any aggregation, and their mean size was ≈3.3 nm, almost constant independent of dopant atoms (Figure S1, Supporting Information). In Figure S2 (Supporting Information), atomic force microscopy (AFM) images also show that typical topographic heights of R-CNDs, N-CNDs, and S-CNDs were mostly between 2.5 and 3.5 nm. This could be attributed to the fact that our capping agent, oleylamine, prevented undesired overreaction and aggregation between the precursors and resulting CNDs.[7] The high-resolution TEM images indicate that our CNDs were mostly amorphous (Figure 2c, inset); however, they partly showed a lattice fringe of 0.24 nm with a very short-range order, which proved the formation of polyaromatic carbon domains (Figure 2d). It was noted that there was no significant difference between the physical structures of our CNDs, and they were commonly composed of polyaromatic carbon domains of six to ten benzene rings surrounded by amorphous carbon networks.[7] This was further identified by the Raman spectra (Figure S3, Supporting Information). The sharp peak was seen at 1442 cm^{-1} in all samples, which was primarily due to the linearly aggregated 6-membered ring systems.[40] The Raman spectra also show the degree of amorphousness of CNDs. Two prominent peaks at 1348 and 1570 cm^{-1} that were related to D and G bands, respectively, could be seen. The intensity ratios of the D and G bands of R-CNDs, N-CNDs, and S-CNDs were 1.33, 1.47, and 1.55, respectively, where the values corresponded to the ratio of sp^3/sp^2 carbons. This indicated that the degree of amorphousness increased with heteroatoms, or heteroatoms would reduce the crystallinity of the carbon structures.

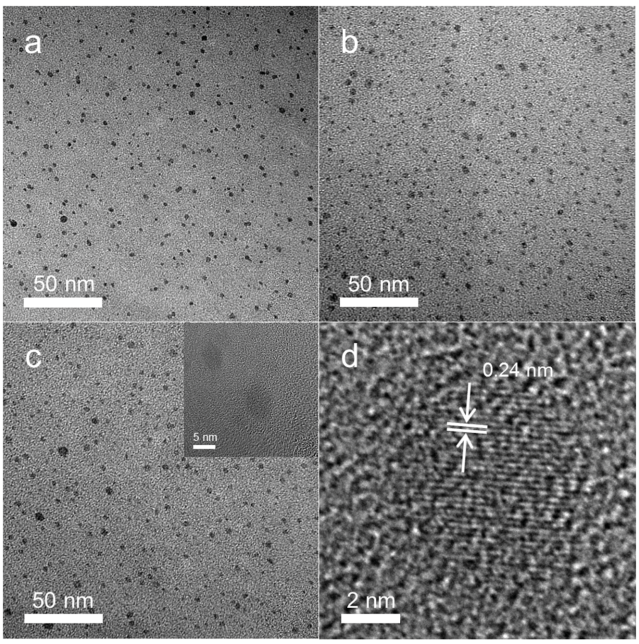

Figure 2. TEM images of a) R-CNDs, b) N-CNDs, and c) S-CNDs. d) High-resolution (HR) TEM images of S-CNDs.

2.3. Chemical Properties of CNDs

To understand the chemical composition of our CNDs, a series of X-ray photoelectron spectroscopy (XPS) was carried out. The full scan XPS spectra, as shown in Figure S4 (Supporting Information), presented three peaks located at 285, 532, and 400 eV, corresponding to C1s, O1s, and N1s, respectively. In the case of S-CNDs, an additional peak at around 167 eV, corresponding to S2p, was also shown in Figure S4c (Supporting Information). This indicated that sulfur atoms exist in only S-CNDs. The atomic ratio of each element, as shown in Table S1 (Supporting Information), showed that there was no critical difference between carbon and oxygen, but the nitrogen content of N-CNDs (7.5899%) is higher than that of R-CNDs (2.1922%) and S-CNDs (2.1877%). This was further identified by the high resolution XPS spectra (**Figure 3**). The high resolution C1s XPS spectra, as shown in Figure 3a–c, show that the C-N peak of N-CNDs was more prominent than that of R-CNDs and S-CNDs, which indicated that more nitrogen atoms were incorporated into the carbon structure. In Figure 3d–f, the N1s XPS spectra were deconvoluted into various kinds of nitrogen-related chemical bonds such as N—C, N—C=O, N=C, and N—O. All of the N1s XPS spectra showed two peaks at 401.04 and 400.4 eV, associated with N—C=O and N—C bondings, respectively, which originated from the oleylamine molecules chemically bonded onto the surface of CNDs. This indicated that the surface states of R-CNDs, N-CNDs, and S-CNDs were identical to each other. However, in Figure 3e, additional two peaks appeared at 401.93 and 399.6 eV, associated with the graphitic N and pyrrolic N, respectively.[29,41,42] These peaks were also identified by carbon-13 nuclear magnetic resonance (^{13}C NMR) data (Figure S5, Supporting Information). Figure S5a (Supporting Information) showed the chemical shifts of 14.06–32.6 (alkyl) and 130.6 ppm (alkene) for the oleyl group and 38.9 ppm for amido carbon, proving the presence of oleylamine molecules.[7] In Figure S5b (Supporting Information), two new peaks were developed at 141.2 and 117.7 ppm, corresponding to the graphitic N and pyrrolic N. Because of these peaks, the intensity of the N1s peak of N-CNDs was higher than that of R-CNDs and S-CNDs, consistent with the results of Table S1 and C1s XPS spectra. Figure 3g–i shows the S2p XPS spectra. We detected no signal in S2p XPS spectra of R-CNDs and N-CNDs (Figure 3g,h); on the other hand, the S2p spectrum of S-CNDs could be deconvoluted into five small peaks centered at 164.05, 165, 166.37, 167.3, and 168 eV. The two peaks at 164.05 and 165 eV, associated with $S2p_{3/2}$ and $S2p_{1/2}$, respectively, originated from spin–orbit coupling of thiophene-S (Figure 3i).[41,43] Additional evidence for these peaks was sought by ^{13}C NMR (Figure S5c, Supporting Information). Figure S5c (Supporting Information) shows the chemical shifts of 137.4–140.9 and 118.7–124.9 ppm related to thiophene-S. In Figure 3i, the other peaks at 166.37, 167.3, and 168 eV originated from oxide S,[43] indicating that sulfur atoms were incorporated into the carbon matrix in two configurations: one is thiophene-S and the other is oxide-S. From the Energy Filtered-TEM image shown in Figure S6 (Supporting Information), we further confirmed the presence of sulfur atoms in the structure of S-CNDs.

In Figure S7 (Supporting Information), infrared (IR) spectra of our CNDs show NH stretching (3500–3000 cm^{-1}), CH stretching (2900–3000 cm^{-1}), and C—N stretching (≈1400 cm^{-1}) bands, which could be attributed to oleylamine molecules on their surface. It is worth noting that in Figure S7b (Supporting Information), the NH stretching peak became prominent, an N—O peak was developed at around 1475–1550 cm^{-1}, and in Figure S7c (Supporting Information), C=S and C—S stretch peaks were detected at around 1050–1400 and 635 cm^{-1}, respectively. These results were consistent with the corresponding XPS data.

2.4. Optical Properties of CNDs

In order to study the optical properties of our CNDs, we carried out UV–visible absorption and PL spectroscopy at room temperature. In Figure S8a (Supporting Information), the absorption spectrum shows a prominent peak at near 250 nm, associated with the $\pi \rightarrow \pi^*$ transition. This peak originated from polyaromatic carbon of 6-membered rings of which $\pi \rightarrow \pi^*$ gap has been known to be about 5.0 eV.[44] Figure S8b (Supporting Information) shows absorption peaks at about 360, 420–470, and 500–560 nm, associated with electronic transitions of heteroatoms (oxygen, nitrogen, sulfur, etc.). The absorption peak at 360 nm was attributed to the $n \rightarrow \pi^*$ transition of the conjugated C=O and C=N bondings.[29,42] All samples showed this peak because a significant amount of oxygen and nitrogen atoms was contained either in the core or on the surface. The absorption band along 420–470 nm was correlated with the $n \rightarrow \pi^*$ transition of the conjugated C=N and C=S bondings[29,32,45,46] and the other band along 500–560 nm corresponded to the $n \rightarrow \pi^*$ transition of the conjugated C=S bonding.[29,32] The latter peak was shown in only S-CNDs because sulfur atoms were incorporated into the carbon core, consistent with the XPS, ^{13}C NMR, and

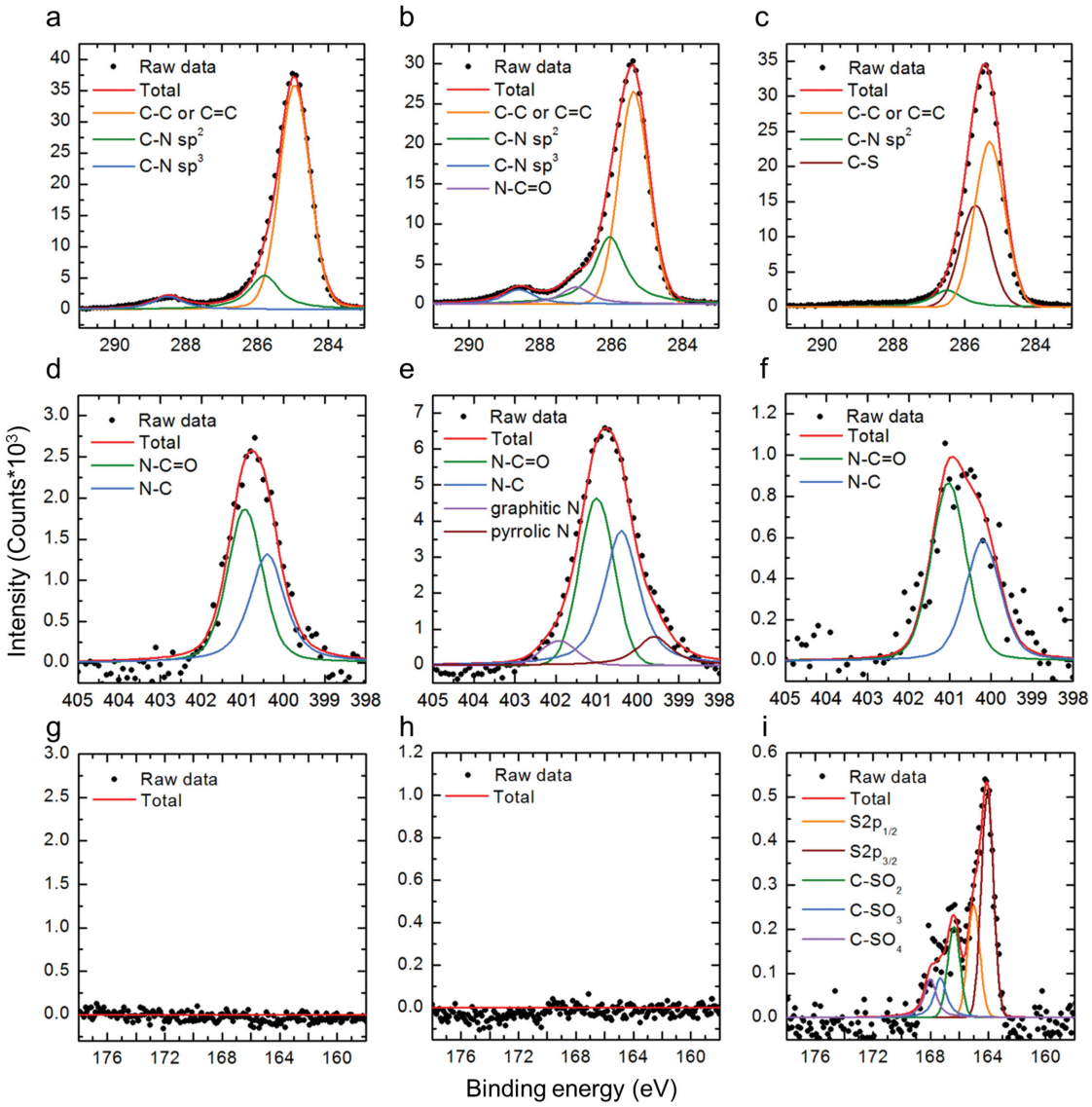

Figure 3. High-resolution XPS data of a–c) C1s, d–f) N1s, and g–i) S2p of a,d,g) R-CNDs, b,e,h) N-CNDs, and c,f,i) S-CNDs.

IR data. Figure S9 (Supporting Information) shows the absorption spectra according to heteroatoms content. We note that the intensity of the absorption peaks at 360 and 420–470 nm was increased with the nitrogen content (Figure S9a,b, Supporting Information); however, in the case of N-CNDs having graphitic N and pyrrolic N, the absorption peaks at 420–470 nm became prominent because of the resonance form of graphitic N and pyrrolic N. The absorption peak at 500–560 nm became more prominent with increasing the sulfur content (Figure S9c,d, Supporting Information).

In **Figure 4**a–c, the excitation maps (a set of excitation spectra) show two bands at the excitation wavelengths of 250 and 360 nm, corresponding to the photon energies of 4.96 and 3.44 eV, respectively. According to UV–visible absorption data, the first (250 nm) and the second band (360 nm) could represent the $\pi \rightarrow \pi^*$ and the $n \rightarrow \pi^*$ transition, respectively. This was also confirmed by the excitation spectra (Figure S10a–c, Supporting Information). Figure 4b,c shows that the excitation peak positions of N-CNDs and S-CNDs were redshifted by 10–25 nm. One plausible explanation for such redshift could be suggested in terms of the heteroatoms, as clarified by the XPS, ^{13}C NMR, and IR data. Nonbonding orbitals of nitrogen and sulfur could be conjugated with the π^* orbitals of the polyaromatic carbon domains in the core of CNDs, and as a result, their conjugation could be extended over more atoms to reduce energy gap (bathochromic shift). The degree of such bathochromic shift of S-CNDs was more pronounced than that of N-CNDs because sulfur has lower electronegativity than nitrogen. Lastly, the broad excitation bands of N-CNDs and S-CNDs were due to a variety of chemical structures with different energy levels derived by nitrogen and sulfur atoms in their carbon core.

In Figure 4d, the emission maps (a set of emission spectra) of R-CNDs show a broad PL band at 420nm regardless of the

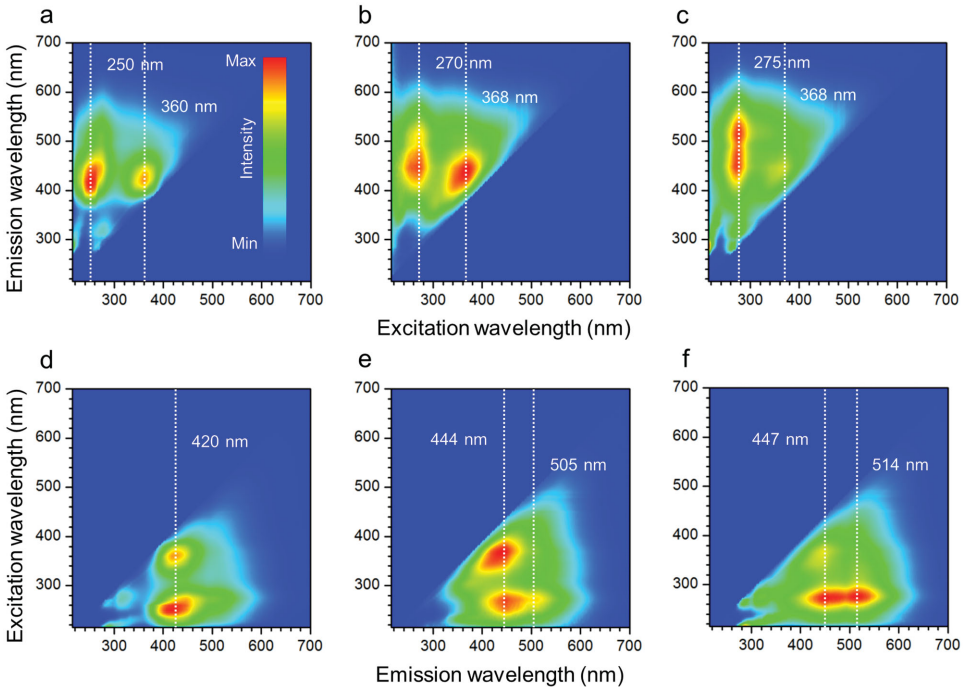

Figure 4. a–c) PL excitation and d–f) emission maps of a,d) R-CNDs, b,e) N-CNDs, and c,f) S-CNDs. The white dotted lines represent the PL peak positions.

excitation wavelength. This was presumably because PL was expected in an appreciable yield only from the lowest excited state, indicating that Kasha's rule was met. Figure 4e,f shows broad PL bands of N-CNDs and S-CNDs at 444 and 447 nm, respectively, which were redshifted by 24–27 nm with respect to R-CNDs, consistent with the excitation spectra. However, in N-CNDs and S-CNDs, there were other broad bands at 505 and 514 nm, respectively, which could be further corroborated by emission spectra (Figure S10d–i, Supporting Information). The PL band of N-CNDs could be deconvoluted into two peaks at around 440 and 505 nm, associated with *n* orbitals of oxygen and nitrogen atoms, respectively.[29] The intensity of the 440 nm peak was much higher than that of the 505 nm peak because of the difference between the oxygen and nitrogen contents, as clarified by the XPS previously. According to the XPS data, the nitrogen content of N-CNDs was higher than that of R-CNDs, so their 505 nm peak intensity could be predominant. Similarly, the PL band of S-CNDs could be deconvoluted into three peaks at around 447, 514, and 575 nm, associated with *n* orbitals of oxygen, nitrogen, and sulfur atoms, respectively. The two PL peaks at 514 and 575 nm arising from nitrogen and sulfur atoms would contribute to generating a PL band at around 520 nm, broadening the PL spectrum to change the color. Such color change could be seen in the photos of our CND solutions taken under 250 and 360 nm UV lamps (Figure S11, Supporting Information).

Figure S12 (Supporting Information) shows that the quantum yields (QYs) of R-CNDs, N-CNDs, and S-CNDs (measured under 360 nm excitation) were 69.87%, 11.51%, and 6.48%, respectively. The QYs were remarkably reduced by doping, presumably due to the fact that heteroatoms would reduce the crystallinity of the carbon core to generate defective sites (radical, etc.), resulting in at least partially quenching PL of our CNDs.[28,47] This was also identified by time-correlated single photon counting (TCSPC) data (Figure S13, Supporting Information). The PL lifetime were obtained by fitting the TCSPC signals to a triple-exponential decay model in Table S2 (Supporting Information). The average lifetimes of N-CNDs (0.157 ns) and S-CNDs (0.155 ns) were lower than that of R-CNDs (4.328 ns). This implied that certain dissipation of photoexcited electrons to lower energy levels would take place in N-CND and S-CND, responsible for broadening their PL spectra. In connection with the QYs, the lifetimes were likewise shortened by 40 times after doping, indicating that dopant atoms (nitrogen and sulfur) would form defective states dissipating and quenching a significant portion of photoexcited electrons.

2.5. Energy Structure of CNDs

Figure S14 (Supporting Information) shows the comparative ultraviolet photoelectron spectroscopy (UPS) data of our CNDs. The secondary cutoff region and Fermi energy were clearly defined (Table S3, Supporting Information) and the highest occupied molecular orbital (HOMO) levels of R-CNDs, N-CNDs, and S-CNDs were calculated to be 6.8, 6.75, and 6.65 eV, respectively. The HOMO level was increased with doping, consistent with the redshifted PL spectra. From the UPS and PL data, the lowest unoccupied molecular orbital (LUMO) levels of R-CNDs, N-CNDs, and S-CNDs could be approximated to be about 3.35, 3.38, and 3.28 eV, respectively. These results were further supported by the cyclic voltammetry and UV–visible absorption spectra (Figure S15 and Table S4, Supporting Information). In Figure S16 (Supporting Information), the Kelvin probe (KP) data show that the Fermi levels of R-CNDs,

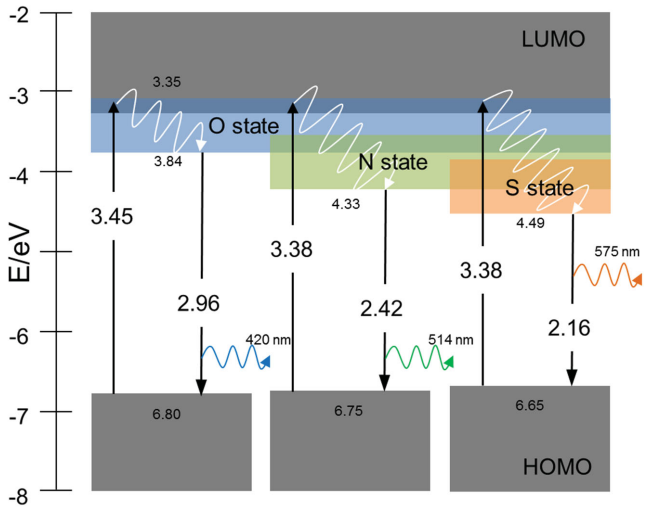

Figure 5. Schematic illustration of the energy structure of our CNDs.

N-CNDs, and S-CNDs were about 4.69, 4.54, and 4.54 eV, respectively. Since the bulk Fermi level of organic semiconductor is assumed to be at the midst of its HOMO-LUMO gap, the HOMO and LUMO levels could be calculated by using KP and PL data.[48] As a result, the HOMO and LUMO levels of R-CNDs, N-CNDs, and S-CNDs were found to be (6.42, 2.97), (6.23, 2.86), and (6.23, 2.86 eV), respectively, consistent with the UPS data (Table S5, Supporting Information). From the above results, in **Figure 5**, a schematic illustration of the electronic structures of our CNDs could be proposed to explain their PL mechanism. There were O, N, and S states, which may be related to the π^* orbital of the C=O, C=N, and C=S bonds as well as HOMO and LUMO, which may be originated from n orbital of the C=O, C=N, and C=S bonds and π^* orbital of the C=C bonds, respectively.[29] In the case of R-CNDs, if the excitation energy is around 3.45 eV, electrons in HOMO can be excited to LUMO. Most of these excited electrons are transferred into the O state via dissipation or phonon generation, and then blue light (420 nm) is emitted by recombination between electrons in the O state and holes in the HOMO. In the meantime, a few of excited electrons are transferred into the N state, and then green light (505 nm) is emitted. In the case of N-CNDs, green light (514 nm), redshifted by 9 nm due to the bathochromic effect, is prominent because the number of the N states is higher than that of R-CNDs. In the case of S-CNDs, sulfur doping induces more S states, energetically below the N state owing to the low electronegativity of sulfur.[29,49] Therefore, S-CNDs can emit intense yellow light (575 nm) arising from their S states.

2.6. EL Devices

Our CNDs have many benefits, such as proper electronic structures, high stability (Figure S17, Supporting Information), and excellent dispersion in common organic solvents (Figure S18, Supporting Information). The solution processability of CNDs will allow low-cost, fast printing process and furthermore flexible forms of devices like solution-processed organic LEDs, which are great merits compared with inorganic GaN-based LEDs. They also have some advantages over comparison with conventional organic emitting materials such as metal–organic complex phosphorescent emitting dopants including rare earth metals (e.g., Tris(2-phenylpyridinato-C2, N)iridium(III) ($Ir(ppy)_3$)), vacuum-deposited organic emitting dopants (e.g., Tris(8-hydroxyquinolinato)aluminum (Alq_3)), and polymeric emitters having issues of batch–batch variation in molecular weight distribution and long synthetic schemes, so that they could be readily used in LEDs in the future if we achieve high brightness and efficiency.[50,51] A schematic of CND-based light-emitting diodes (CND-LEDs) is shown in **Figure 6**a. The device consisted of a patterned Indium Tin Oxide (ITO) anode, a gradient hole injection layer (GraHIL, poly(3,4-ethylenedioxythiophene):poly(styrene sulfonate) (PEDOT:PSS):tetra-fluoroethylene-perfluoro-3,6-dioxa-4-methyl-7-octene-sulfonic acid copolymer (PFI)) (≈40 nm)[52] which have gradually increasing work-function from bottom surface (≈5.2 eV) to top surface (≈5.95 eV), an emitting layer (EML) (≈40 nm) mixed with three materials: tris(N-carbazolyl) triphenylamine (TCTA) as a hole transport host, 1,3,5-tris(N-phenylbenzimidizol-2-yl)benzene (TPBI) as electron transport host emissive host, and CNDs as a emissive dopant for 5:5:1 weight ratio, respectively, a TPBI (≈50 nm) as electron transport layer, a lithium fluoride (LiF) (≈1 nm) and aluminum (≈100 nm) as the cathode. The electronic structure of CND-LEDs was proposed in Figure 6b; gradient work-function of GraHIL can facilitate hole injection to the HOMO level of TCTA host and co-host system in the EML, and can improve the device efficiency by facilitating the energy transfer from host to CND dopants and broadening the recombination zone.[52–54]

Figure 6c showed the normalized EL spectra of CND-LEDs at the fixed bias of 13 V. Although the EL peak positions of all samples were the same (480 nm), they exhibited broad EL bands in the range from 500 to 700 nm in the case of N-CND and S-CND based LEDs. This might be caused by a higher density of the N and S states of N-CNDs and S-CNDs than R-CNDs, consistent with the absorption and PL data. N-CND and S-CND based LEDs also showed broader EL spectrum than R-CND based LEDs at every applied bias, and the EL spectrum did not change with applied bias. This indicates that co-host system in the EML can efficiently facilitate energy transfer from host to CND dopants and induce the EL spectrum from CND dopants solely (Figure S19, Supporting Information). Figure 6d shows that the CIE (Commission Internationale d'Éclairage) coordinates of R-CND, N-CND, and S-CND based LEDs were (0.2298, 0.2866), (0.2698, 0.3320), and (0.2894, 0.3351), respectively. This indicated that the CIE coordinates were redshifted with doping nitrogen and sulfur atoms, or in other words, increasing the density of the N and S state. Especially, the CIE coordinate of S-CND based LEDs was very close to that of the pure white light (0.33, 0.33) because of their more panchromatic EL spectrum. In Figure 6e,f, and Figure S20 (Supporting Information), R-CND based LEDs showed higher current efficiency (≈1.65 cd A^{-1}), external quantum efficiency (EQE) (≈0.6%), and maximum luminance (≈80 cd m^{-2}) than N-CND based OLEDs (≈0.36 cd A^{-1}, ≈0.19%, and ≈34 cd m^{-2}, respectively) and S-CND based OLEDs (≈0.39 cd A^{-1}, ≈0.2%,

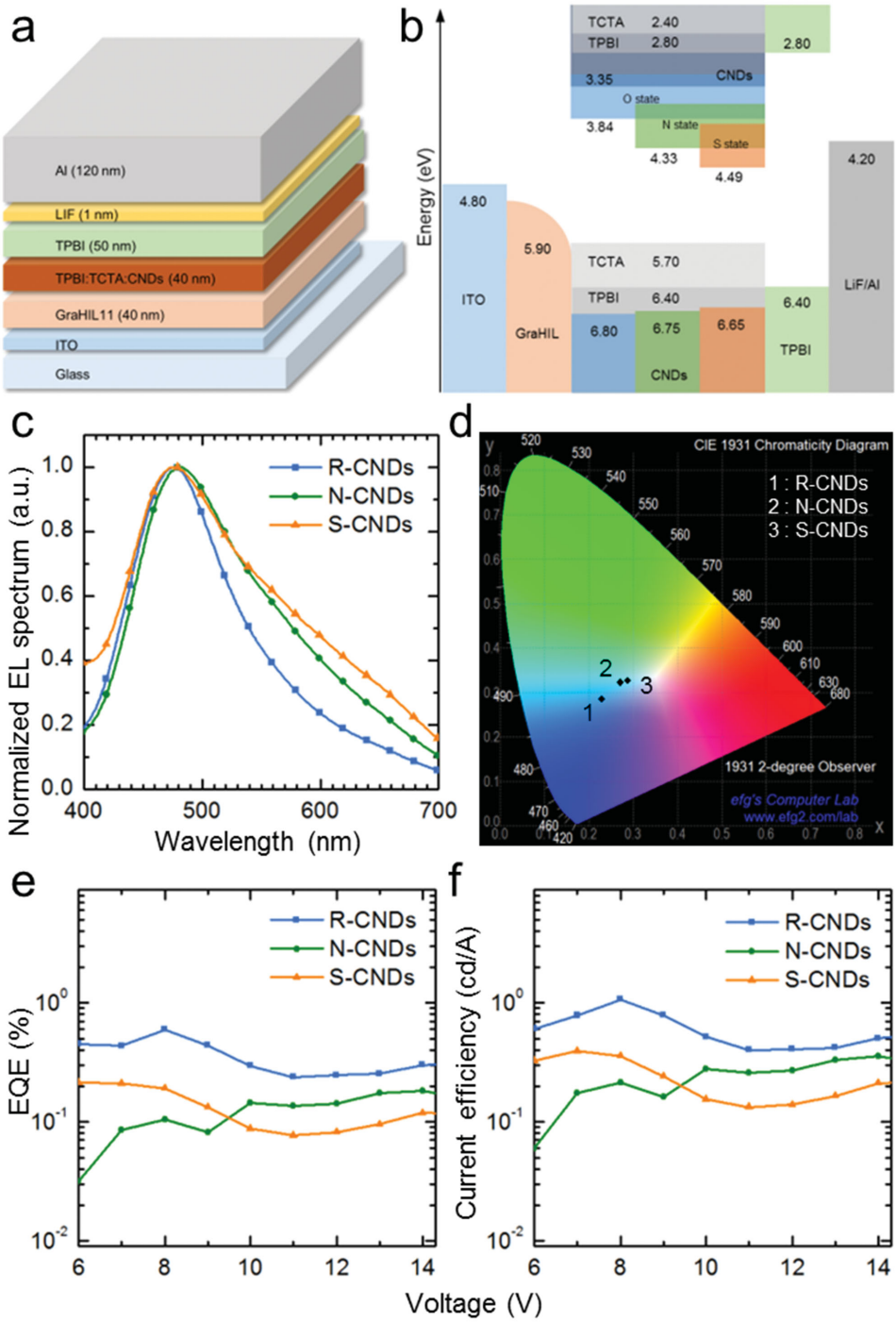

Figure 6. a) Physical and b) electronic structures of LEDs employing our CNDs. c) Normalized EL spectra of CND-LEDs at the fixed bias of 14 V. d) CIE chromaticity coordinates calculated from the EL spectra. e) External quantum efficiency (EQE) and f) current efficiency of LEDs employing R-CND, N-CNDs, and S-CNDs.

and ≈29 cd m^{-2}, respectively). It was worth noting that the EQEs of N-CND and S-CND based LEDs were lower than that of R-CND based LEDs, presumably due to the fact that the EQE of LEDs is directly related with the radiative quantum efficiency of the light-emitting dopants (Equation (S1), Supporting Information).[55]

3. Conclusions

In Summary, we have synthesized nitrogen and sulfur doped CNDs through the carbonization of single molecular precursors: EDDA and ETDA. TEM images and Raman analyses showed that no significant physical change was led in CNDs

by doping, but the degree of amorphousness increased with doping, indicating that dopants would reduce the crystallinity of the carbon core. A series of spectroscopies measurements showed that by doping, absorption bands were developed at near 450 and 550 nm and the PL spectra were redshifted and broadened into a longer-wavelength region. From the UPS and KP data, the electronic structure of our CNDs could be proposed to explain the PL mechanism. Since our CNDs have proper electronic structure, high stability, and excellent solubility in common organic solvents, we have successfully demonstrated CND-LEDs. Such CND-LEDs exhibited broad, panchromatic EL ranging from 400 to 700 nm to produce bright white light and CIE coordinate (0.2894, 0.3351). These results showed not only the efficient doping strategy but also unprecedented pure white light of CND-LEDs. Thus, we believe that this study could shed light on understanding the effect of doping on the optical properties of CNDs in a molecular level and future applications of the CND-related optoelectronics.

4. Experimental Section

Synthesis of CNDs: 3 g of citric acid was added to 3 mL of water (5 M) in order to prepare carbon source. For synthesis of nitrogen or sulfur doped CNDs, EDDA and ETDA were used as nitrogen and sulfur sources, respectively, instead of citric acid. The mixture was vigorously stirred to dissolve source materials in water and then injected into oil phase made by mixing 1 mL of oleylamine and 9 mL of octadecene in a 3-neck round bottom flask. This solution was vigorously stirred under argon atmosphere for 10 min to form a milky emulsion. The emulsion was heated to 250 °C for 2 h. The color of the solution became transparent during raising temperature and then finally turned into dark brown solution at 250 °C. After cooled to room temperature, the resultant solution was purified with methanol through the method of centrifugation (3000 rpm for 10 min). This process was repeated three times to remove residuals. The final product was dried in a vacuum oven (80 °C) for 2 d and then redispersed in hexane or toluene for further use.

Sample Preparation and Characterizations: For TEM, 1 mg of sample was dissolved in l mL of hexane (1 mg mL^{-1}) and then dropped onto a CF300-Cu grid (Electron Microscopy Sciences). TEM was performed using Jeol JEM-2200FS with the image Cs-corrector at an accelerating voltage of 200 kV. For XPS, 10 mg of sample was dissolved in 1 mL of hexane (10 mg mL^{-1}) and then this solution was spin cast onto a 50 nm Au-coated silicon substrate. XPS was performed using an Escalab 250 spectrometer with an Al X-ray source (1486.6 eV). For ^{13}C NMR, more than 100 mg of sample was dissolved in 1 mL of chloroform-d (>100 mg mL^{-1}) and then this solution was transferred to an NMR sample tube (600 MHz) and sealed by Teflon tapes. ^{13}C NMR spectra were obtained by Bruker DRX500. For IR spectroscopy, 100 mg of sample was dissolved in 1 mL of anhydrous toluene (100 mg mL^{-1}), and then 100 µL of this solution was dropped onto a KBr window (Pike Technologies), dried for 12 h under high-purity nitrogen flow and sandwiched with another KBr window. IR was carried out using a Nicolet 6700 FT-IR spectrometer. For UV–visible absorption and PL spectroscopy, 0.4 mg of sample was dissolved in 4 mL of hexane (0.1 mg mL^{-1}), and then this solution was transferred to a 10 mm cuvette. UV–vis absorption spectra were obtained on a Mecasys Optizen POP spectrophotometer. PL spectra were derived by a Jasco FP-8500 fluorometer. Current–voltage–luminance (*I–V–L*) characteristics were measured by using a Minolta CS2000 spectroradiometer with Keithley236 source.

Fabrication of Light-Emitting Diodes: ITO-patterned glass was sonicated in acetone and 2-isopropanol for 15 min each, and boiled in 2-isopropanol. After cleaning, it was UV-ozone treated for 20 min to make the ITO surface hydrophilic and remove the residues. After these steps, GraHIL (PEDOT:PSS:PFI in 1:1 weight ratio) was spin-coated to give the 40 nm film and then baked for 30 min at 150 °C. Then, the solution containing various series of doped CND dopants, hole transporting TCTA, and electron transporting TPBI in 1:5:5 weight ratio in tetrahydrofuran solvent were spin-coated on top of the GraHIL film in ambient condition to give the 50 nm thick EML. Then, electron transporting TPBI (50 nm), LiF, and aluminum (100 nm) were sequentially deposited in thermal evaporator under high vacuum (<10^{-7} Torr).

Supporting Information

Supporting Information is available from the Wiley Online Library or from the author.

Acknowledgements

S. Do, W. Kwon, and Y.-H. Kim. contributed equally to this work. This work was supported by Samsung Research Funding Center of Samsung Electronics under Grant No. SRFC-MA1401-07. The authors thank Hyun-Jin Park (National Institute for Nanomaterials Technology) for assistance with TEM. S. Do is also very grateful to Eunho Lee and Donghun Sin (POSTECH) for their help with Raman spectroscopy and AFM, respectively.

Received: September 2, 2015
Revised: October 16, 2015
Published online: November 19, 2015

[1] S. N. Baker, G. A. Baker, *Angew. Chem. Int. Ed.* **2010**, *49*, 6726.
[2] Y. P. Sun, B. Zhou, Y. Lin, W. Wang, K. A. S. Fernando, P. Pathak, M. J. Meziani, B. A. Harruff, X. Wang, H. Wang, P. G. Luo, H. Yang, M. E. Kose, B. Chen, L. M. Veca, S. Y. Xie, *J. Am. Chem. Soc.* **2006**, *128*, 7756.
[3] H. Li, Z. Kang, Y. Liu, S.-T. Lee, *J. Mater. Chem.* **2012**, *22*, 24230.
[4] S. Sahu, B. Behera, T. K. Maiti, S. Mohapatra, *Chem. Commun.* **2012**, *48*, 8835.
[5] H. Li, X. He, Z. Kang, H. Huang, Y. Liu, J. Liu, J. Liu, S. Lian, C. H. A. Tsang, X. Yang, S.-T. Lee, *Angew. Chem. Int. Ed.* **2010**, *49*, 4430.
[6] L. Li, G. Wu, G. Yang, J. Peng, J. Zhao, J.-J. Zhu, *Nanoscale* **2013**, *5*, 4015.
[7] W. Kwon, G. Lee, S. Do, T. Joo, S.-W. Rhee, *Small* **2014**, *10*, 506.
[8] S.-L. Hu, K.-Y. Niu, J. Sun, J. Yang, N.-Q. Zhao, X.-W. Du, *J. Mater. Chem.* **2009**, *19*, 484.
[9] J. Shen, Y. Zhu, C. Chen, X. Yang, C. Li, *Chem. Commun.* **2011**, *47*, 2580.
[10] L. Zheng, Y. Chi, Y. Dong, J. Liu, B. Wang, *J. Am. Chem. Soc.* **2009**, *131*, 4564.
[11] D. Pan, J. Zhang, Z. Li, C. Wu, X. Yan, M. Wu, *Chem. Commun.* **2010**, *46*, 3681.
[12] W. Kwon, S.-W. Rhee, *Chem. Commun.* **2012**, *48*, 5256.
[13] S. Liu, J. Tian, L. Wang, Y. Luo, J. Zhai, X. Sun, *J. Mater. Chem.* **2011**, *21*, 11726.
[14] W. Kwon, S. Do, S.-W. Rhee, *RSC Adv.* **2012**, *2*, 11223.
[15] L. A. Ponomarenko, F. Schedin, M. I. Katsnelson, R. Yang, E. W. Hill, K. S. Novoselov, A. K. Geim, *Science* **2008**, *320*, 356.
[16] L. S. Li, X. Yan, *J. Phys. Chem. Lett.* **2010**, *1*, 2572.
[17] S. J. Zhu, J. H. Zhang, C. Y. Qiao, S. J. Tang, Y. F. Li, W. J. Yuan, B. Li, L. Tian, F. Liu, R. Hu, H. N. Gao, H. T. Wei, H. Zhang, H. C. Sun, B. Yang, *Chem. Commun.* **2011**, *47*, 6858.
[18] W. Wei, C. Xu, L. Wu, J. Wang, J. Ren, X. Qu, *Sci. Rep.* **2014**, *4*, 3564.

[19] Z. L. Wu, P. Zhang, M. X. Gao, C. F. Liu, W. Wang, F. Leng, C. Z. Huang, *J. Mater. Chem. B* **2013**, *1*, 2868.
[20] Y. Wang, L. Dong, R. Xiong, A. Hu, *J. Mater. Chem. C* **2013**, *1*, 7731.
[21] Q. Li, S. Zhang, L. Dai, L.-S. Li, *J. Am. Chem. Soc.* **2012**, *134*, 18932.
[22] Y.-Q. Zhang, D.-K. Ma, Y. Zhuang, X. Zhang, W. Chen, L.-L. Hong, Q.-X. Yan, K. Yu, S.-M. Huang, *J. Mater. Chem.* **2012**, *22*, 16714.
[23] Z. Yang, M. Xu, Y. Liu, F. He, F. Gao, Y. Su, H. Wei, Y. Zhang, *Nanoscale* **2014**, *6*, 1890.
[24] Y. Li, Y. Zhao, H. Cheng, Y. Hu, G. Shi, L. Dai, L. Qu, *J. Am. Chem. Soc.* **2012**, *134*, 15.
[25] W. Li, Z. Zhang, B. Kong, S. Feng, J. Wang, L. Wang, J. Yang, F. Zhang, P. Wu, D. Zhao, *Angew. Chem. Int. Ed.* **2013**, *52*, 1.
[26] J. Liu, X. Liu, H. Luo, Y. Gao, *RSC Adv.* **2014**, *4*, 7648.
[27] Z. Li, H. Yu, T. Bian, Y. Zhao, C. Zhou, L. Shang, Y. Liu, L.-Z. Wu, C.-H. Tung, T. Zhang, *J. Mater. Chem. C* **2015**, *3*, 1922.
[28] S. Do, W. Kwon, S.-W. Rhee, *J. Mater. Chem. C* **2014**, *2*, 4221.
[29] D. Qu, Z. Sun, M. Zheng, J. Li, Y. Zhang, G. Zhang, H. Zhao, X. Liu, Z. Xie, *Adv. Optical Mater.* **2015**, *3*, 360.
[30] W. Kwon, J. Lim, J. Lee, T. Park, S.-W. Rhee, *J. Mater. Chem. C* **2013**, *1*, 2002.
[31] H. Ding, J.-S. Wei, H.-M. Xiong, *Nanoscale* **2014**, *6*, 13817.
[32] D. Qu, M. Zheng, P. Du, Y. Zhou, L. Zhang, D. Li, H. Tan, Z. Zhao, Z. Xie, Z. Sun, *Nanoscale* **2013**, *5*, 12272.
[33] H. Huang, Y.-C. Lu, A.-J. Wang, J.-H. Liu, J.-R. Chen, J.-J. Feng, *RSC Adv.* **2014**, *4*, 11872.
[34] Y. Sun, C. Shen, J. Wang, Y. Lu, *RSC Adv.* **2015**, *5*, 16368.
[35] Y.-C. Lu, J. Chen, A.-J. Wang, N. Bao, J.-J. Feng, W. Wang, L. Shao, *J. Mater. Chem. C* **2015**, *3*, 73.
[36] C. Xu, Q. Han, Y. Zhao, L. Wang, Y. Li, L. Qu, *J. Mater. Chem. A* **2015**, *3*, 1841.
[37] Y. Dong, H. Pang, H. B. Yang, C. Guo, J. Shao, Y. Chi, C. M. Li, T. Yu, *Angew. Chem. Int. Ed.* **2013**, *52*, 7800.
[38] X. Li, S. P. Lau, L. Tang, R. Ji, P. Yang, *Nanoscale* **2014**, *6*, 5323.
[39] A. Oberlin, *Carbon* **1984**, *22*, 521.
[40] R. N. Tarrant, O. Warschkow, D. R. McKenzie, *Vibrational Spectrosc.* **2006**, *41*, 232.
[41] W. Lu, X. Qin, S. Liu, G. Chang, Y. Zhang, Y. Luo, A. M. Asiri, A. O. Al-Youbi, X. Sun, *Anal. Chem.* **2012**, *84*, 5351.
[42] D. Qu, M. Zheng, L. Zhang, H. Zhao, Z. Xie, X. Jing, R. E. Haddad, H. Fan, Z. Sun, *Sci. Rep.* **2014**, *4*, 5294.
[43] S. Yang, L. Zhi, K. Tang, X. Feng, J. Maier, K. Mullen, *Adv. Funct. Mater.* **2012**, *22*, 3634.
[44] A. R. Matamala, A. A. Alarcón, *Int. J. Quantum Chem.* **2012**, *112*, 1316.
[45] E. M. Genies, A. Boyle, M. Lapkowski, C. Tsintavis, *Synth. Met.* **1990**, *36*, 139.
[46] W. Wu, L. Zhan, W. Fan, J. Song, X. Li, Z. Li, R. Wang, J. Zhang, J. Zheng, M. Wu, H. Zeng, *Angew. Chem. Int. Ed.* **2015**, *54*, 6540.
[47] R. Misra, B. Dhokale, T. Jadhav, S. Mobin, *Dalton Trans.* **2014**, *43*, 4854.
[48] H. Ishii, N. Hayashi, E. Ito, Y. Washizu, K. Sugi, Y. Kimura, M. Niwano, Y. Ouchi, K. Seki, *Phys. Status Solidi A* **2004**, *201*, 1075.
[49] S. Yang, J. Sun, X. Li, W. Zhou, Z. Wang, P. He, G. Ding, X. Xie, Z. Kang, M. Jiang, *J. Mater. Chem. A* **2014**, *2*, 8660.
[50] X. Li, M. Rui, J. Song, Z. Shen, H. Zeng, *Adv. Funct. Mater.* **2015**, *25*, 4929.
[51] X. Li, Y. Liu, X. Song, H. Wang, H. Gu, H. Zeng, *Angew. Chem. Int. Ed.* **2015**, *54*, 1759.
[52] a) T.-W. Lee, Y. Chung, O. Kwon, J.-J. Park, *Adv. Funct. Mater.* **2007**, *17*, 390; b) M.-R. Choi, T.-H. Han, K.-G. Lim, S.-H. Woo, D. H. Huh, T.-W. Lee, *Angew. Chem. Int. Ed.* **2011**, *50*, 6274; c) T.-H. Han, Y. Lee, M.-R. Choi, S.-H. Woo, S.-H. Bae, B. H. Hong, J.-H. Ahn, T.-W. Lee, *Nat. Photon.* **2012**, *6*, 105; d) T.-H. Han, M.-R. Choi, S.-H. Woo, S.-Y. Min, C.-L. Lee, T.-W. Lee, *Adv. Mater.* **2012**, *24*, 1487; e) K.-G. Lim, H.-B. Kim, J. Jeong, H. Kim, J. Y. Kim, T.-W. Lee, *Adv. Mater.* **2014**, *26*, 6461.
[53] W. Kwon, Y.-H. Kim, C.-L. Lee, M. Lee, H. C. Choi, T.-W. Lee, S.-W. Rhee, *Nano Lett.* **2014**, *14*, 1306.
[54] Y.-H. Kim, H. Cho, J. H. Heo, T.-S. Kim, N. Myung, C.-L. Lee, S. H. Im, T.-W. Lee, *Adv. Mater.* **2015**, *27*, 1248.
[55] H. Nakanotani, T. Higuchi, T. Furukawa, K. Masui, K. Morimoto, M. Numata, H. Tanaka, Y. Sagara, T. Yasuda, C. Adachi, *Nat. Commun.* **2014**, *5*, 4016.